Cellular and Molecular Biology
E-ISSN : 1165-158X / P-ISSN : 0145-5680
www.cellmolbiol.org

# Investigation on antimicrobial, antioxidant, and anti-cancerous activity of *Agaricus bisporus* derived β-Glucan against cervical cancer cell line

Ankita Bhosale[1#], Rashmi Trivedi[1#], Tarun Kumar Upadhyay[1#*], Dhruvi Gurjar[1#], Faranak Aghaz[2], Fahad Khan[3], Pratibha Pandey[3], Md. Zeyaullah[4], Md. Shane Alam[5], Mohammad A A Al-Najjar[6], Samra Siddiqui[7]

[1] Department of Biotechnology, Parul Institute of Applied Sciences and Centre of Research for Development, Parul University, Vadodara, Gujarat, 391760, India
[2] Nano Drug Delivery Research Center, Faculty of Pharmacy, Health Technology Institute, Kermanshah University of Medical Sciences, Kermanshah, Iran
[3] Department of Biotechnology, Noida Institute of Engineering & Technology, Greater Noida, 201306, India
[4] Department of Basic Medical Science, College of Applied Medical Sciences, Khamis Mushayt Campus, King Khalid University (KKU), Abha, KSA.
[5] Department of Medical Laboratory Technology, College of Applied Medical Sciences, Jazan University, Jazan, KSA.
[6] Department of pharmaceutical sciences and pharmaceutics. Faculty of Pharmacy, Applied Science Private University, Amman. Jordan.
[7] Department Health Services Management, College of Public Health and Health Informatics, University of Hail, Hail P.O. Box 2240, Saudi Arabia

[#] All authors have equally contributed

**ARTICLE INFO**

***Original paper***

***Article history:***
*Received: July 21, 2022*
*Accepted: September14, 2022*
*Published: September 30, 2022*

***Keywords:***

*Antioxidant, antifungal, antibacterial, lysosomal accumulation, mitochondrial membrane potential, agaricus bisporus, JC-1 aggregation*

**ABSTRACT**

Cervical cancer is one of the leading causes of death among women. Due to incomplete knowledge and hidden symptoms, it is not easily diagnosable. After the diagnosis of cervical cancer at an advanced stage, treatment such as chemotherapy and radiation therapy become too much costly along with having many side effects such as hair loss, loss of appetite, nausea, tiredness, etc. β-Glucan does a novel polysaccharide has many immunomodulatory properties. In our research, we have tested the efficacy of *Agaricus bisporus* derived β-Glucan particles (ADGPs) as an antimicrobial, antioxidant and anticancer agent against the cervical cancer HeLa cells. Prepared particles were quantified for carbohydrate content by anthrone test and further HPTLC analysis to confirm the polysaccharide nature and 1,3 glycosidic linkages of β-Glucan. ADGPs were found to have efficient antimicrobial activity against various fungal and bacterial tested strains. DPPH assay confirmed the antioxidant activity of ADGPs. Cell viability was assessed against the cervical cancer cell line by using the MTT and $IC_{50}$ was found at 54µg/ml. Furthermore, β-Glucan was found to induce a significant amount of ROS, leading to the apoptosis of cells. The same was also assessed with the help of Propidium Iodide (PI) staining. With the help of JC-1 staining, β-Glucan was found to disrupt the Mitochondrial Membrane Potential (MMP), ultimately resulting in the cancer cell HeLa death. Based on our experimental findings, we found that ADGPs can be proven as an efficient therapy for cervical cancer treatment and work as an antimicrobial and antioxidant agent.

**Doi:** http://dx.doi.org/10.14715/cmb/2022.68.9.24 

## Introduction

Medicinal mushrooms are frequently used in a wide range of fields, including dietary foods nutritious auxiliary products, and health (1). Mushrooms such as the button mushroom (*Agaricus bisporus*), golden oak mushroom (*Lentinula edodes*), Oyster mushroom (*Pleurotus* and specifically *Plerotus ostreatus*), enoki or golden needle mushroom (*Flammulina velutipes*), the Jew's ear or wood ear mushroom (*Auricularia auricula-judae)*, maitake (*Grifola frondosa*), are becoming a popular alternative of many therapeutics (2). In Asian regions, they are used for promoting and maintaining a good state of health. Antimicrobial, anti-inflammatory, immunomodulatory, antidiabetic, cytotoxic, inhibitor, hepatoprotective, anticancer, inhibitor, antiallergic, antihyperlipidemic, and prebiotic activities are documented for medicinal mushrooms (3-5). Various mushrooms have been demonstrated to have a wide range of specialized medical properties and due to their efficient medicinal and therapeutic values; they have attracted a lot of attention from researchers and scientists. Many of them are already in use, particularly in medicine, for their immunomodulatory properties and to improve traditional treatments by increasing their effectiveness and lowering side effects. *Agaricus bisporus* mushroom is rich in β-Glucans, ergosterol, ergothioneine, and vitamin D. Because of conjugated linoleic acid activity, it is found that *A. bisporus* can be included in the diet to prevent prostate cancer. It was already reported in our previous studies that *Agaricus bisporus* has chemical composition (moisture, ash, protein, carbohydrate, total fat) and minerals composition (Se, Ni, Mn, Cu, Zn, Na, N, Fe, P, Ca, Mg, S, and K) and its nutritional, medicinal profile and quality categorization (53). Previously the detection of the heavy

* Corresponding author. Email: tarun_bioinfo@yahoo.co.in

metal concentration among fresh fruiting bodies of *A. bisporus* was performed by (54) which play very vital role in dietary intake studies.

Mushrooms are a good source for the extraction of antimicrobial compounds that can work as antibiotics. These antimicrobial compounds are present as secondary metabolites and needed for their growth and reproduction (6). In a study, mushroom β-glucan isolated from edible, wild, natural and cultured mushrooms was found to show an efficient antimicrobial activity against *S.aureus, S.marcenses, E.faecalis, S.marcenses* and *P.aeruginosa* (7). β-Glucan obtained from mushrooms has various phenolic, terpenoids, steroid and polyketide compounds which give them strong antioxidant activities. These antioxidant effects can help in various therapeutics, including cancer and heart diseases (8). In a study, mushroom extracts inhibited the growth of prostate cancer in athymic mice, indicating an antiproliferative and proapoptotic effect. The nephroprotective effects of *P. ostreatus* and *A. bisporus* liquid extracts on hyperoxaluria-induced urolithiasis in Wistar rats were studied after 0.75 percent (v/v) ethylene glycol was added to the drinking for nine weeks (9-12).

*Cervical cancer* is the cancer of the cervix and is the fourth leading cause of death among women worldwide (13). Cervical cancer mortality has been steady for the past four decades, despite encouraging improvements in screening and prevention. More than 90% of cases of cervical cancer occur in low- and middle-income nations, where cervical cancer screening and interference programs are not widely implemented (14). Cervical cancer can be treated by various therapies, including surgery, such as girdle lymphadenectomy and radical hysterectomy, radiation therapy, and chemotherapy (15). Current cervical cancer treatment options include radical hysterectomy or definitive chemo-radiation, depending on the clinical stage of the disease (16). These treatments of cancer, such as chemotherapy and radiation therapy may result in menopause, infertility, and side effects of these therapies may affect not only cancer cells but also rapidly dividing cells in systems throughout the body. There is a need to develop efficient therapies for cancer through the use of natural compounds. Moreover, Synthetic antibiotics and antimicrobial agents pose a threat to human health, so exploring naturally occurring compounds as antimicrobial agents are necessary. In our study, we have tried to elucidate the impact of *A. bisporus* derived β-Glucan (ADGPs) as an antimicrobial, antioxidant and anticancer agent on cervical cancer cells.

## Materials and Methods

### Reagents and chemicals

Anthrone reagent (Thermo Scientific), Sulfuricacid (HiMedia), n-Butyl alcohol (HiMedia), Methanol (HiMedia), DPPH (2,2-Diphenyl-1-picrylhydrazyl) (Sigma-Aldrich), 3-(4,5-dimethylthiazol-2-yl)-2,5-diphenyl tetrazolium bromide (MTT) (Invitrogen), ($H_2$DCFDA) (dichlorofluoresceindiacetate) (Invitrogen), LysoTracker RedDND99 (Invitrogen), JC-1 (Invitrogen), Hoechst (Invitrogen), FBS, Antibiotic-antimycotic solution, Dulbecco's Modified Eagle Medium (DMEM) (Gibco), Trypsin (HiMedia).

### Cell culture maintenance

Cervical cancer cell line HeLa was purchased from National Centre for Cell Science (NCCS, Pune). Cells were maintained in sterile conditions having humidified environment with 5% $CO_2$ in a $CO_2$ incubator. The media used was Dulbecco's Modified Eagle Medium (DMEM), which was supplemented with 10% Fatal Bovine Serum (FBS) and 1% Antibiotic and Antimycotic solution (Gibco).

### Glucan particle preparation

*A.bisporus* was purchased from the local market of Vadodara, Gujarat. 100 g of the fruiting bodies were taken and washed with distilled water (DW). The fruiting bodies were crushed with the help of a mortar pestle. To form a more continuous paste, a homogenizer was used for 10 minutes. The crushed fruiting bodies were added to 200 ml of DW and boiled in a water bath for 30 minutes at 90°C. After boiling, it was centrifuged in a cooling centrifuge at 9,000 rpm for 10 minutes. The supernatant obtained was discarded, and the obtained pellet was washed with 80% ethanol. Further, the sample was again incubated for 4 hours in a water bath at 90°C. After incubation, Sample was centrifuged at 9000 rpm for 10 minutes. Obtained pellet was resuspended in DW and pH adjusted from 4 to 5 by using Hydrochloric acid and further kept for incubation at 70°C for 30 minutes. The incubated sample was centrifuged at 8000 rpm for 10 minutes at 4°C. Obtained pellet was first two times washed with isopropanol followed by Acetone wash (Twice). Pellet was further transferred into a Petri plate and kept for air drying. The obtained powder was filtered with the muslin cloth and stored (17, 18).

### β-Glucan size analysis

The Malvern Mastersizer was used to analyze the particle size of prepared ADGPs. Malvern Master Sizer can be used for dry and wet samples, producing accurate and quick results (19). Particle size was determined using the laser diffraction technique. The samples were distributed using a liquid or air cell. A laser beam passed through the cell, scattering light through the distributed particles and causing a scattering pattern to appear. The particle size distribution was calculated using the Mie theory, based on the angles and intensities of scattered light detected using optics.

### Quantitative estimation of carbohydrates through Anthrone test

To perform the anthrone test, we followed the previously described protocol (20). Briefly, Anthrone Reagent was made by dissolving 0.2 g of Anthrone in 100mL of concentrated $H_2SO_4$. 10 µL of glucose stock solution (1mg/1ml) was diluted in 100ml of distilled water to make a glucose working solution. Glucose samples were taken in 200, 400, and 600µg/ml, along with one unknown concentration sample of the ADGPs. 4mL of the anthrone reagent was added to each sample. Further, samples were incubated for 30 minutes at 90°C in a water bath with cotton caps on the tubes. After incubation, samples were cooled to room temperature a notable variation in the color of the solution was detected after the sample cooled down. After observing the physiological test, a qualitative test was performed by measuring the absorbance with the help of Readwell Robonik ELISA Plate Reader at 630 nm.

### FTIR analysis

Fourier transform infrared spectrometry that is FTIR is a technique that is used to get an infrared spectrum that

helps in the identification of functional groups and linkages present in the compound. To study the absorbance of β-Glucan particles, the procedure was performed by following the previously described protocol (21). The analysis was performed with Bruker alpha FTIR where the particles were kept on a diamond crystal and analyzed with 32 scans averaged at a resolution of 4 $cm^{-1}$. The obtained graph was compared with previously defined spectra.

**HPTLC analysis**

On 10x10 cm glass-supported silica gel HPTLC plates, the HPTLC analysis was performed. The samples and standard were applied to the HPTLC plate using an Automatic TLC Sampler 4 (ATS4) (CAMAG) equipped with a Hamilton Gastight Syringe (25 mL; 1700 Series) at a rate of 160 nL/s. 2 µL of β-glucan and D-glucose with concentrations of 5 and 10 mg/mL were separated using HPLC-grade*n*-butanol/methanol/water (50:25:20) as mobile phase. The plate was developed in a preliminarily impregnated automatic developing chamber-2 (ADC-2) linear ascending mode for 20 minutes at room temperature. CAMAG TLC scanner IV was utilized to scan the produced and derivatized plate in the visible region at 254 nm wavelength in absorbance mode. The slit confines were 4.00 X 0.45 mm, and the scanning speed was 20 mm per second (22).

**Antimicrobial activity**

The antimicrobial activity of the β-Glucan was determined with the help of a previously described protocol. Agar well diffusion method was employed for the antimicrobial susceptibility testing. 100 ml of agar media was sterilized, cooled and inoculated with 0.1 ml of bacterial suspensions of *E.coli*, *S.pyogenus*, *P.aeruginosa, and S.aureus* and fungal strains *C.albicans, A.niger, and A.clavatus*. The inoculated suspensions were mixed well and poured into sterilized Petri plates for the solidification of the agar media. After solidification, with the help of a cork borer, about 6 mm diameter was punched and 100µl sample of β-Glucan in various concentrations (5, 25, 50, 100, 250, and 500µg/ml) were added in different wells. In control well, distilled water was added and the inoculated Petri plates were incubated at 37°C for 24 h and the zone of inhibition was measured (23).

**Antioxidant activity**

Antioxidant activity was assessed by the previously described protocol with the DPPH reagent. In brief, 0.2mM DPPH reagent was made by dissolving DPPH in methanol and 4 ml of DPPH was added in 1 ml of β-Glucan (200, 400, 600 and 800µg/ml) and kept for incubation in the dark at room temperature for 20 min. After incubation, absorbance was taken at 517nm with a BioTek SynergyH1 microplate reader (24).The %free radical scavenging activity was calculated by using the following equation:

$$\frac{\text{Absorbance of controloplate reader}}{\text{Absorbance of control}} \times 100$$

Where control is DPPH+methanol.

**Cell viability assay**

HeLa cells were seeded in 96 well plates with 10,000 cells in each well. The cells were treated with 10, 20, 30, 40, 50, and 60µg/ml. Treatment of the cells was performed in a triplicate manner and incubated for 24 hours at 37°C in a 5% $CO_2$ incubator. After incubation, the cells were stained with 5mg/mL and incubated for 4 hours in the dark with 5% $CO_2$ (25). After incubation gets over, MTT produced formazan crystals as which were dissolved by treating the cells with DMSO. The absorbance was measured with an ELISA plate reader at a wavelength of 570 nm. % Viability was calculated according to the given equation

$$\%\text{Viability} = \left(\frac{\text{Absorbance of treatment}}{\text{Absorbance of control}}\right) X100$$

**Reactive Oxygen Species generation**

Reactive oxygen species (ROS) are naturally produced by metabolic activities of mitochondria and play an important role in cellular signaling, but increased amounts of ROS are harmful to the cells, tissues, and body as an increased amount of ROS generation can ultimately lead to cell death.

There are many factors, including changes in oxidative phosphorylation (OXPHOS), transition metal ions, oxidase activity, protein folding, thymidine, and polyamine catabolism that can induce ROS generation. To assess the ROS generation in HeLa cells by ADGPs, $1x10^5$cells per well were seeded in a 12 well plate and, after overnight incubation, treated with 50, 100, and 150µg/ml doses of ADGPs and incubated for 24 hours at 37°C with 5%CO2. After the incubation period was over, cells were stained with DCFH-DA Dye. This staining was performed according to the previously described protocol (26). After staining, the cells were incubated for 30 min in the dark and further washed with PBS. Cells were observed in a fluorescent microscope and photographed.

**Hoechst staining**

Hoechst staining was performed according to the previously described protocol (27) to observe morphological changes and nuclear fragmentation in HeLa cells after treatment with ADGPs. Briefly, 1x105 cells were seeded in 12 well plates and left overnight for growth and proliferation. Further, cells were treated with different dosages of β-Glucan (50, 100, and 150µg/ml) and incubated for 24 hours. After incubation, cells were stained with Hoechst dye at 37°C for 30 minutes in the dark. Nuclear morphological changes were examined under a fluorescent microscope.

**Propidium Iodide staining**

PI staining was performed to determine the apoptosis of the HeLa cells in response to the ADGPs treatment. $1x10^5$ cells were seeded in 12 well plates and left overnight for growth and proliferation and further cells were treated with 50, 100, and 150µg/ml with ADGPs and incubated for 24 hours at 37°C in a CO2 incubator. When the incubation period was finished, cells were stained with PI (1mg/ml DW) and incubated for 5 min in the dark. This staining was performed according to the previously described protocol (28). After incubation gets over, cells were washed with PBS and visualized under a fluorescent microscope EVOS FLoid Imaging System, Thermo Fisher Scientific.

**Change in mitochondrial membrane potential (JC-1 staining)**

JC-1 (5, 5, 6, 6'-tetrachloro-1,1',3,3' tetraethylbenzimidazoylcarbocyanine iodide) dye is used to identify changes in mitochondrial membrane potential (MMP). Cells

($1x10^5$) were seeded in 12 well plates and incubated for 24 hours. The cells were further treated with 50, 100, and 150µg/ml of ADGPs and again incubated for 24 hours at 37°C in a CO2 incubator. When the incubation period was over, cells were stained with JC-1 dye. This staining was performed according to the previously described protocol (29). After staining, cells were incubated for 15 minutes in the dark in a CO2 incubator at 37°C. After incubation, cells were washed with PBS and imaged in red and green fluorescence under a fluorescent microscope.

### LysoTracker

LysoTracker Red DND-99 is a red-fluorescent dye for labelling and tracking acidic organelles in live cells. LysoTracker Red DND-99 becomes protonated and therefore is markedly sequestrated in the lysosomes of the cells. Lysosomal acidity plays an important role in the accumulation of LysoTracker within this acidic organelle; its visible light intensity could be a sign of lysosomal pH alterations (30). Cells ($1x10^5$) were seeded in 12 well plates to observe lysosome activity and incubated for 24 hours. The cells were treated with 50, 100, and 150µg/ml of ADGPs and incubated for 24 hours at 37°C in a CO2 incubator. Once the time was over, cells were stained with LysoTracker Red DND-99 dye and further kept for 30 min in the dark. After staining, cells were visualized under a fluorescence microscope (31).

## Results

### Extraction of β-glucan particle

The obtained β-Glucan particles from the fruiting bodies of *Agaricus bisporus* possesses were slightly brown in colour, as shown in Figure 1.

### β-Glucan particle size analysis

ADGPs were analyzed with Malvern Mastersizer and the average diameter of the particles was found 563 nm. β-Glucan with a size range of 2–4 µm which can be easily phagocytosed by the cells (32). In our study, Particle size was around 563 nm as shown in (Figure 2), which can be considered particles that can be easily phagocytosed by the cells. Moreover, the PDI (polydispersity index) value which is the representation of the particle size distribution or average homogeneity of the particles was 0.587. A higher PDI value means particles are less homogenous and have large size distribution of particles. PDI value less than <0.4 indicates narrow size distribution (33) and in our test, it was 0.587, indicating particles are almost homogenous in nature (34).

**Figure 1.** Extracted β-Glucan particle.

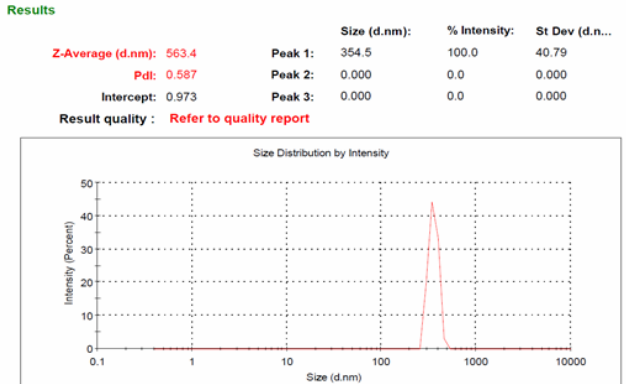


**Figure 2.** Physiochemical characterization of β-Glucan by Malvern mastersizer instrument.The average particle size distribution was found to be around 563nm.

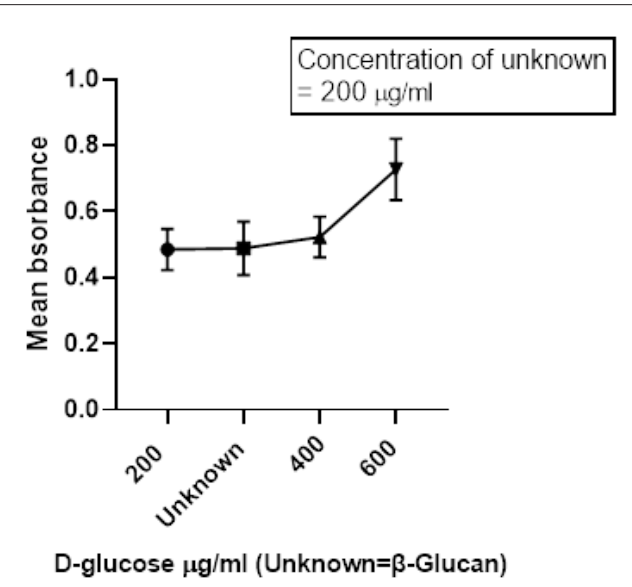


**Figure 3.** Carbohydrate content estimation of ADGPs with the help of anthrone test. The concentration of the unknown sample was 200µg/ml.

### Quantitative estimation of polysaccharide by Anthrone test

The anthrone test was used to estimate carbohydrate content. When conc. $H_2SO_4$ dehydrates carbohydrates. Furfural is produced. Anthranol, the enol tautomer of anthrone, is the active form of the reagent, which reacts with the carbohydrate furfural derivative to produce a bluish-green color complex. In the Anthrone test, we found the concentration of an unknown (ADGPs) sample of 200µg/ml, as shown in Figure 3.

### Characterization with FTIR

The FTIR spectra of obtained ADGPs have their main peaks at 3284, 3000, 1632, 1377, 994, 556 and 514 $cm^{-1}$.In a study, Deniz et al., 2018 confirmed the nature of β-Glucan from *Agaricus bisporus* by the transmittance spectra. They found that peaks at 3600 to 3200 $cm^{-1}$indicated O-H stretch of polysaccharide. The peak at approximately 3000-2700

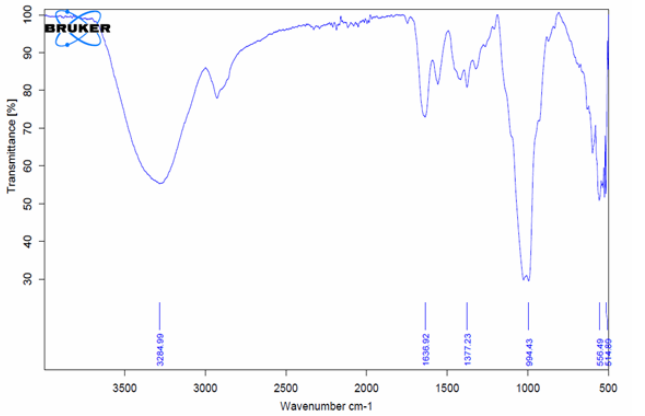


**Figure 4.** FTIR Transmittance spectra of ADGPs with the help of Bruker alpha instrument. It was found to show maximum peaks at 3284, 3000, 1632, 1377, 994, 556 and 514cm$^{-1}$ indicating that it has OH, CHOH, CO stretch and β-linkage.

cm$^{-1}$ corresponds to C-H stretch which is indicating that the tested material (β-Glucan) is a carbohydrate. An almost similar pattern was observed in our absorption spectra, indicating that the material is β-Glucan, as shown in Figure 4 (35).

## HPTLC analysis

HPTLC analysis showed D-Glucose as the major polysaccharide fraction present in ADGPs (Figure 5). D-Glucose was taken as standard and β-Glucan showed similar peaks as seen in D-Glucose. HPTLC analysis was performed with the help of a CAMAG Application System (Muttenz, Switzerland). The developed silica plate was visualized at 254 nm wavelength.

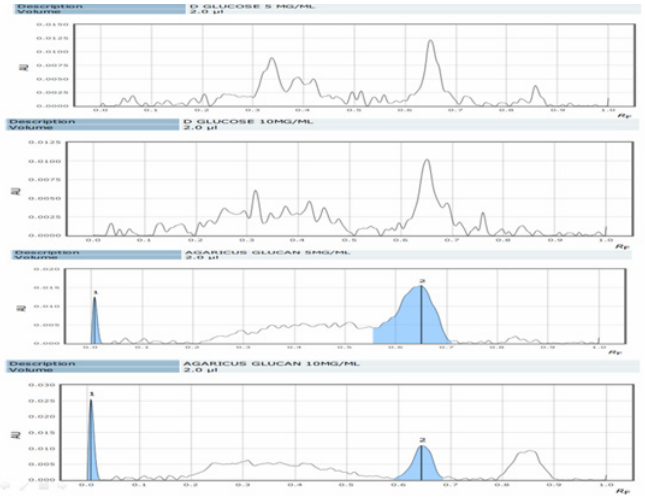

**Figure 5.** HPTLC spectra of D-Glucose and β-Glucan. Both D-Glucose and β-Glucan were taken in 5 and 10mg/ml and peaks of both the samples were seen at retention factor (RF) 0.6-0.7, confirming the presence of polysaccharide content in β-Glucan.

## Antimicrobial activity

Efficient antibacterial activity was shown by ADGPs. At 500µg/ml concentration of ADGPs, the zone of inhibition was highest for all the tested strains (Table 1). Comparative MIC for all the standard drugs and ADGPs are shown in (Table 2). There was no clear zone of inhibition seen at 5µg/ml for both ADGPs and standard strains. Maximum zone of inhibition 21 was found for *S.aureus* and *S.pyogenus* at 500µg/ml concentration. Antifungal activity of β-Glucan (Table 3) and MIC was found 1000µg/ml for each *C.albicans*, *A.niger*, and *A.clavatus*.

**Table 1**. Zone of inhibition for standard strains and ADGPs.

| Standard Strain | Zone of Inhibition ADGPs(µg/ml) | | | | | | Standard | | | | | |
|---|---|---|---|---|---|---|---|---|---|---|---|---|
| | 5 | 25 | 50 | 100 | 250 | 500 | 5 | 25 | 50 | 100 | 250 | 500 |
| ***E.coli* [MTCC443]** | - | 11 | 13 | 15 | 17 | 19 | - | 20 | 23 | 28 | 28 | 28 |
| ***P.aeruginosa* [MTCC 1688]** | - | 13 | 14 | 16 | 17 | 20 | - | 20 | 23 | 24 | 26 | 27 |
| ***S.aureus* [MTCC 96]** | - | 13 | 15 | 17 | 18 | 21 | - | 17 | 19 | 21 | 22 | 22 |
| ***S.pyogenus* [MTCC 442]** | - | 12 | 14 | 15 | 19 | 21 | - | 16 | 19 | 21 | 21 | 22 |
| ***C.albicans* [MTCC 227]** | - | 12 | 15 | 16 | 18 | 20 | - | 18 | 21 | 22 | 22 | 24 |

**Table 2**. Minimum Inhibitory Concentrations of ADGPs and standard drugs. MIC varied in the range of 50-125µg/ml.

| ADGPs | | Minimum Inhibitory concentration | | | |
|---|---|---|---|---|---|
| | | ***E.coli*** **MTCC443** **125** | ***P.aeruginosa*** **MTCC 1688** **62.5** | ***S.aureus*** **MTCC 96** **50** | ***S.pyogenus*** **MTCC 442** **100** |
| **Antibacterial Standard Drugs** | Gentamycin | 0.05 | 1 | 0.25 | 0.5 |
| | Amphicilin | 100 | 100 | 250 | 100 |
| | Chloramphenicol | 50 | 50 | 50 | 50 |
| | Ciprofloxacin | 25 | 25 | 50 | 50 |
| | Norfloxacin | 10 | 10 | 10 | 10 |

**Table 3.** Antifungal activity of the β-Glucan.

| ADGPs | | Minimum Inhibitory concentration | | |
|---|---|---|---|---|
| | | **C.albicans** **MTCC 227** **1000** | **A.niger** **MTCC 282** **1000** | **A.clavatus** **MTCC 1323** **1000** |
| **standard drugs** | **Nystatin** | 100 | 100 | 100 |
| | **Greseofulvin** | 500 | 100 | 100 |

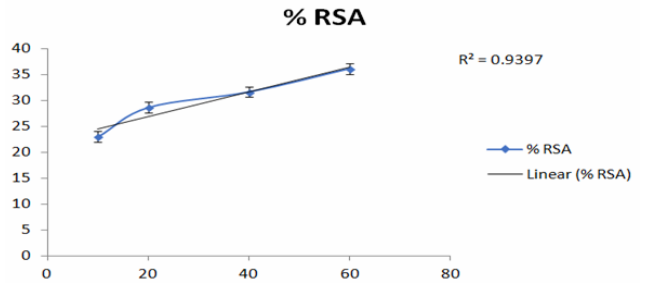


**Figure 6.** ADGPs showed a dose-dependent increase in radical scavenging activity (RSA) and a maximum % RSA was reported at 80µg/ml.

### Antioxidant activity

ADGPs were found to show efficient antioxidant activity (Figure 6). The antioxidant activity of ADGPs was found to increase with the increase in concentration. β-Glucan neutralizes DPPH free radical by giving an electron to it and turning the purple color solution into a creamy solution.

### Cell viability assessment through MTT

Cell viability of the cells treated with the ADGPs was found to decrease with an increase in the concentration of the treatment. Maximum cell viability was found at the concentration of 10µg/ml, while maximum cytotoxicity was found at 60µg/ml (Figure 7). $IC_{50}$ of the treatment dose was 54µg/ml indicating mortality of half of the cells.

### Reactive Oxygen Species generation indicates cell death

Reactive oxygen species (ROS) can induce damage to cellular components, including DNA, RNA, lipids, and proteins leading to the apoptosis of the cell. Normal healthy cells possess various defence mechanisms to combat the bad effects of ROS; still, an inadequate amount of ROS generation can lead to oxidative stress resulting in cell death (36). Intracellular ROS can oxidise DCFHDA (non-fluorescent) to DCF (fluorescent). In our test, the level of ROS assessed with the help of increasing fluorescence and it was found to increase in a concentration-dependent manner indicating apoptosis of the HeLa cells (Figure 8a). Fluorescence intensity was analyzed with the help of GraphPad Prism and ImageJ softwares. All the values were found to be highly significant, with a *p-value* of less than 0.0001, as shown in (Figure 8b).

### Detection of nuclear fragmentation by Hoechst staining

Hoechst dye is specific for the nucleus of the cells and it stains both live and apoptotic cell nuclei with the broken cell membrane. Morphological changes caused due to the effect of various doses of the treatment can e easily observed with the help of Hoechst staining (37). In our study, cells were treated with 50, 100, and 150µg/ml concentrations of the ADGPs and apoptotic cells were observed by the condensed and fragmented nuclei of the cells. Maximum morphological changes were observed at 150µg/ml of the treatment concentration of the ADGPs (Figure 9).

### Apoptosis detection by Propidium iodide staining

PI intercalates with nucleic acids by intercalating between the bases of double-stranded DNA with little or

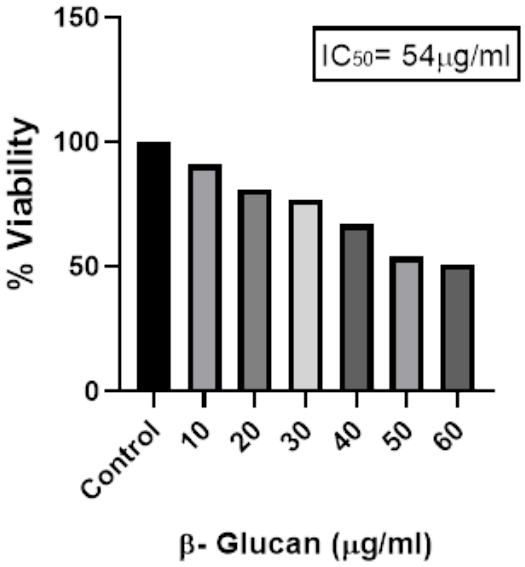


**Figure 7.** ADGPs showed a dose-dependent increase in radical scavenging activity (RSA) and a maximum % RSA was reported at 80µg/ml.

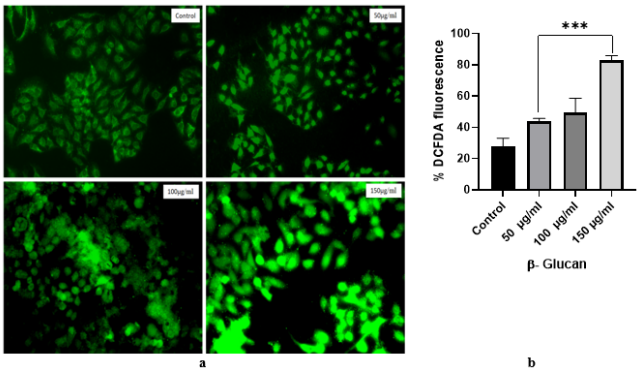


**Figure 8.** Intracellular ROS generation in HeLa cells after the treatment with different doses of 50,100,150µg/ml of ADGPs for 24h. (a) Fluorescence intensity increased with the concentration and it was highest at 150µg/ml, indicating maximum cell death. (b) Statistical analysis shows all values significant with *p<0.0001*.

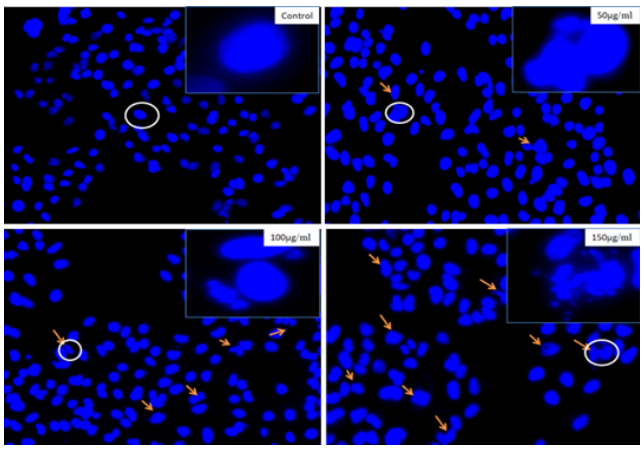


**Figure 9.** Hoechst stain showing the fragmentation of the nuclei. In control well with no treatment. Nuclei are almost oval with intact membranes. With the increase in the concentration, nuclear fragmentation can be observed. Maximum changes were observed at150µg/ml treatment concentration of the ADGPs.

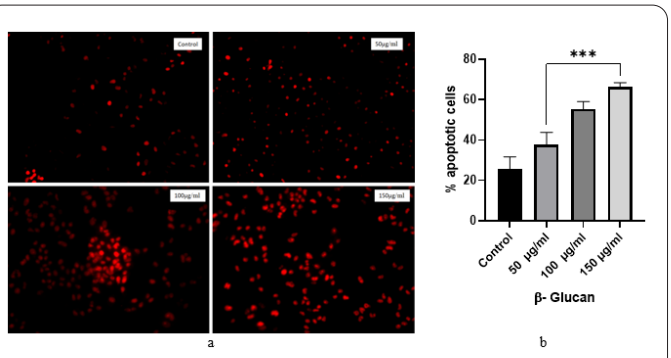


**Figure 10.** (a) Propidium iodide staining showed efficient apoptosis of the HeLa cells in a dose-dependent manner. (b) Statistical analysis with $p<0.0001$.

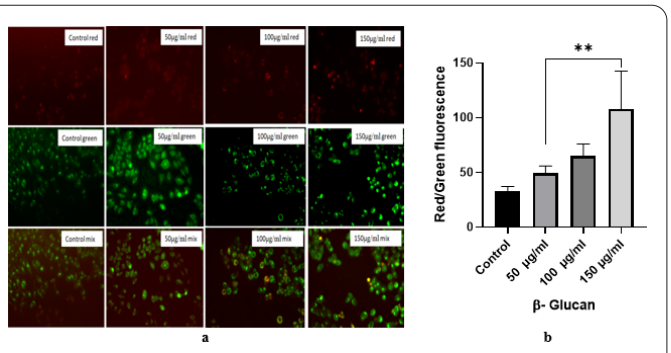


**Figure 11.** (a) JC-1 staining of HeLa cells showing the disruption of mitochondria leading to cellular death. (b) Statistical analysis of merged colour fluorescence images with *p value* 0.0061.

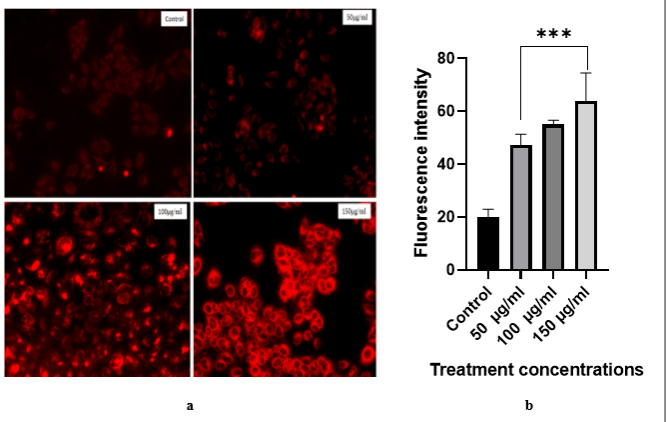


**Figure 12.** (a) LysoTracker staining in HeLa cell with treatment concentration 50,100,150µg/ml of ADGPs. Increased fluorescence intensity is indicative of pH alteration and autophagy induction (b) Statistical analysis with the help of one-way ANOVA showing all values significant with $p<.005$.

no sequence preference, allowing it to readily permeate cells with compromised cell membranes (28). PI cannot pass through intact cell membranes and give intense fluorescence when it reaches the nucleus of cells with the disrupted cell membranes. In our test, the fluorescence intensity was found to increase with the increase in treatment concentration as shown in (Figure 10a). The highest fluorescence was found at 150µg/ml, indicating maximum cell death. One-way ANOVA analysis showed all the significant values (Figure 10b).

**Mitochondrial membrane potential analysis through JC-1 staining**

JC dye is used to measure mitochondrial membrane potential in healthy and apoptotic cells in a variety of cells. JC-1 is a lipophilic cationic dye with a natural green fluorescence. This dye, when it enters mitochondria, starts accumulating in a concentration-dependent manner and forms reversible red-colored J aggregates (38). In healthy cells, due to the more negative potential of mitochondria, JC-1 aggregates well and show efficient red fluorescence. In apoptotic cells, due to the increase in mitochondrial membrane potential (less negative), JC-1 accumulation in mitochondria is not very well and the dye remains in its monomeric green form. In our study, we have found an efficient increase in red and green fluorescence in red and green fluorescence with the increase in the concentration of treatment (Figure 11a). Merged images of red and green fluorescence show the disruption of the mitochondria in the treated cells. Merged red and green fluorescence images (somewhat yellow to orange coloration) were used for the statistical analysis and showed a significant $p<0.5$ value (Figure 11b).

**Determination of apoptosis by tracking disrupted acidic organelles through LysoTracker Red DND-99 staining**

LysoTracker Red accumulates in the lysosomal compartment of the cell due to alteration in the pH of the lysosomes resulting in increased fluorescence intensity. In our study, there was an increase in fluorescence intensity found with the increase in the concentration of the ADGPs treatment (Figure 12a).One-way ANOVA analysis showed that all values were found to be significant (Figure 12b).

**Discussion**

Mushrooms such as button mushroom (*Agaricus bisporus*), shiitake (*Lentinula edodes*), oyster mushroom (specifically *Pleurotus ostreatus*), enoki or golden needle mushroom (*Flammulina velutipes*), the Jew's ear or wood ear mushroom (*Auricularia auricula-judae*), maitake (*Grifola frondosa*) and others are eaten because of their nutritional and culinary worth. In this study, we have tried to evaluate the anticancer potential of ADGPs. The size of the prepared particles was analyzed with the help of a Malvern mastersizer and it was found to be 563 nm. It is reported that a particle size of 1–2 µm has better adsorbent capability than many large sizes of particles (39). So, prepared particles were found in the range of phagocytic uptake values. In our study, we have used the anthrone test, which gives a bluish-green color complex and indicates the presence of carbohydrates in the ADGPs. The same procedure was also reported by Pillai et al., (2014) (40) for the quantitative estimation of polysaccharides. Hassan et al., (2015) (41) found the FTIR spectra peaks of ADGPs at 3463, 2927, 2367, 1664, and 833 $cm^{-1}$. In our study, we have also found peaks at 3262 and 2920 $cm^{-1}$ showing a similar pattern to the reference spectra. In our study, ADGPs were found to show an efficient antibacterial activity with minimum inhibitory concentrations of 125, 62.5, 50, and 100 for *E.coli*, *S.pyogenus*, *P.aeruginosa, and S.aureus,* respectively, which was in correlation with the study performed by Volman et al., 2008 (42), who reported an efficient antimicrobial activity of ADGPs against several fungal and bacterial strains. In one more study, efficient antimicrobial activity of ADGPs was reported using test

organisms *S. aureus*, MRSA, *K. pneumoniae, P. aeruginosa*, and *C. albicans* and reported a similar pattern obtained in our study(43). The antioxidant activity of ADGPs was found to increase with the increase in concentration. The antioxidant activity of ADGPs was also reported by (44). Cell viability was assessed with the help of tetrazolium dye MTT and IC50 was reported 54µg/ml cell viability was found to decrease in a concentration-dependent manner. In a study, it was reported that potential β-Glucan-derived nanoparticles were tested against cervical cancer cells and IC50 was found at 50µg/ml (45). Intracellular Reactive oxygen species generation is harmful if they are produced in an uncontrolled increased concentration and ultimately lead to cell death. ROS generation is a part of the natural aerobic respiration and metabolism of the cells and it plays a very important role in the proper functioning of the various cellular processes (46). We have found ROS generation in a concentration-dependent manner in HeLa cells which is indicative that ADGPs could be proven as potent anticancer agents. Wu et al., (2021) (47) observed β-Glucan leading to respiratory bursts due to excess ROS generation. In a study, the antitumor activity of β-Glucan was reported in a ROS-dependent manner (48). Furthermore, nuclear morphology was observed with Hoechst staining and apoptotic cells were identified with condensed and fragmented nuclei. A similar finding was also reported in a study in which it was shown that round nuclei and fragmented nuclei corresponded to viable and apoptotic cells, respectively (49). Apoptosis detection in HeLa cells was also observed with the help of PI staining that is only permeable to apoptotic cells with a disintegrated nucleus (50). We have found a dose-dependent increase in apoptosis in HeLa cells. Moreover, alteration in mitochondrial membrane potential was assessed by JC-1 dye. Mitochondrial disintegration leads to the suppression of ATP production resulting in a decrease in energy supply to the cell that ultimately leads to cell death (38). In our study, we have found that JC-1 dye was not able to accumulate well within mitochondria due to the disintegration of the mitochondrial membrane, which is a clear indication of cell death. Furthermore, the disintegration of acidic organelles was detected with the help of LysoTracker Red DND-99. Lysosomes are organelles having acidic pH (3.5-6.0) and maintain various functions, including digestion and degradation of macromolecules. Disturbance in the function of lysosomal activity can also cause several diseases (51, 52). In our study, it was found that a dose-dependent increase in the fluorescence intensity of LysoTracker stained cells indicated apoptosis of cells due to phagocytosis.

In the present study, we have tried to evaluate the anticancerous potential of ADGPs. *Agaricus bisporus* mushrooms have been found to possess many antimicrobial, antioxidant, and anticancerous activities. We found that ADGPs can be used as an efficient antimicrobial, antioxidant and anticancer agent for cervical cancer as it showed efficient ROS generation and change in mitochondrial membrane potential along with alteration in pH of the acidic organelles. The further potential of ADGPs needs to explore to make it a therapeutic treatment for cervical cancer.

**Acknowledgements**
The authors are thankful to Chairperson & Medical Director (Dr. Geetika Madan Patel) and Team CR4D.This research study was funded by the Centre of Research for Development, Parul University, Vadodara, in the form of Intra Mural Research Project (CR4D/IMSL/046) for conducting this research. The authors are also thankful to Microcare Laboratory, Surat, for the analysis of the sample for antimicrobial activity.

**Interest conflict**
The authors declare no conflict of interest.

**Consent for publications**
The author read and approved the final manuscript for publication.

**Availability of data and material**
All data generated during this study are included in this published article

**Authors' Contribution**
All authors had significantly contributed to the manuscript. Tarun Kumar Upadhyay designed the concept, Ankita wrote the initial draft, and Rashmi, Ankita and Dhruvi performed the experiment. Data analysis, reviewing, and editing all other authors contributed.

**Ethics approval and consent to participate**
Ethical review and approval were waived for this study due to the severity level of the applied procedure, which is defined as "Not an experiment" according to the ethical statement.

**References**

1. Lindequist U. The merit of medicinal mushrooms from a pharmaceutical point of view. Int J Med Mushrooms. 2013;15(6).
2. Miao YZ, Lin Q, Cao Y, He GH, Qiao DR, Cao Y. Extraction of water-soluble polysaccharides (WSPS) from Chinese truffle and its application in frozen yogurt. Carbohydr. Polym. 2011;86(2):566-73.
3. Elkhateeb WA. What medicinal mushroom can do. Chem Res J. 2020;5(1):106-18.
4. Spelman K, Sutherland E, Bagade A. Neurological activity of Lion's mane (*Hericium erinaceus*). J. Restor. Med. 2017;6(1):19-26.
5. Jeitler M, Michalsen A, Frings D, Hübner M, Fischer M, Koppold-Liebscher DA, Murthy V, Kessler CS. Significance of medicinal mushrooms in integrative oncology: A narrative review. Front Pharmacol. 2020;11:580656.
6. Akyuz M, ONGANER A, Erecevit P, Kirbag S. Antimicrobial activity of some edible mushrooms in the eastern and southeast Anatolia region of Turkey. Gazi Univ. J. Sci. 2010;23(2):125-30.
7. Özcan Ö, Ertan F. Beta-glucan content, antioxidant and antimicrobial activities of some edible mushroom species. Food Sci. Technol. 2018;6(2):47-55.
8. Puttaraju NG, Venkateshaiah SU, Dharmesh SM, Urs SM, Somasundaram R. Antioxidant activity of indigenous edible mushrooms. J. Agric. Food Chem. 2006;54(26):9764-72.
9. Adams LS, Chen S, Phung S, Wu X, Ki L. White button mushroom (*Agaricus bisporus*) exhibits antiproliferative and proapoptotic properties and inhibits prostate tumor growth in athymic mice. Nutr. Cancer. 2008;60(6):744-56.
10. Ahmed OM, Ebaid H, El-Nahass ES, Ragab M, Alhazza IM. Nephroprotective effect of *Pleurotus ostreatus* and *Agaricus bisporus* extracts and carvedilol on ethylene glycol-induced uroli-

thiasis: roles of NF-κB, p53, bcl-2, bax and bak. Biomolecules. 2020;10(9):1317.
11. Elisashvili VI. Submerged cultivation of medicinal mushrooms: bioprocesses and products. Int. J. Med. Mushrooms. 2012;14(3).
12. Blumfield M, Abbott K, Duve E, Cassettari T, Marshall S, Fayet-Moore F. Examining the health effects and bioactive components in Agaricus bisporus mushrooms: A scoping review. J. Nutr. Biochem. 2020;84:108453.
13. Urasa M, Darj E. Knowledge of cervical cancer and screening practices of nurses at a regional hospital in Tanzania. Afr. Health Sci. 2011;11(1).
14. WHO. Cervical cancer. https://www.who.int/cancer/prevention/diagnosis-screening/cervical-cancer/en/. Published 2018. Last accessed on March 18, 2019.
15. Kim JY, Byun SJ, Kim YS, Nam JH. Disease courses in patients with residual tumor following concurrent chemoradiotherapy for locally advanced cervical cancer. Gynecol. Oncol. 2017;144(1):34-9.
16. Cohen PA, Jhingran A, Oaknin A, Denny L. Cervical cancer. Lancet. 2019;393(10167):169-182.
17. Rahar S, Swami G, Nagpal N, Nagpal MA, Singh GS. Preparation, characterization, and biological properties of β-glucans. J Adv Pharm Technol Res. 2011;2(2):94-103.
18. Guizani N, Rahman MS, Klibi M, Al-Rawahi A, Bornaz S. Thermal characteristics of Agaricus bisporus mushroom: freezing point, glass transition, and maximal-freeze-concentration condition. Int. Food Res. J. 2013;20(4).
19. Heo TY, Kim YN, Park IB, Lee DU. Amplification of Vitamin D2 in the White Button Mushroom (Agaricus bisporus) by UV-B Irradiation and Jet-Milling for Its Potential Use as a Functional Ingredient. Foods. 2020;9(11):1713.
20. Haldar D, Sen D, Gayen K. Development of spectrophotometric method for the analysis of multi-component carbohydrate mixture of different moieties. Appl. Biochem. Biotechnol. 2017;181(4):1416-34.
21. Ban Z, Horev B, Rutenberg R, Danay O, Bilbao C, McHugh T, Rodov V, Poverenov E. Efficient production of fungal chitosan utilizing an advanced freeze-thawing method; quality and activity studies. Food Hydrocoll. 2018;81:380-8.
22. Han SS, Cho CK, Lee YW, Yoo HS. Antimetastatic and immunomodulating effect of water extracts from various mushrooms. J Acupunct Meridian Stud. 2009;2(3):218-27.
23. Pratap GM, Manoj KM, Sai SA, Sujatha B, Sreedevi E. Evaluation of three medicinal plants for anti-microbial activity. Ayu. 2012;33(3):423.
24. Khan AA, Gani A, Shah A, Masoodi FA, Hussain PR, Wani IA, Khanday FA. Effect of γ-irradiation on structural, functional and antioxidant properties of β-glucan extracted from button mushroom (*Agaricus bisporus*). Innov Food Sci Emerg Technol. 2015;31:123-30.
25. Kaminari A, Nikoli E, Athanasopoulos A, Sakellis E, Sideratou Z, Tsiourvas D. Engineering mitochondriotropic carbon dots for targeting cancer cells. Pharmaceuticals. 2021;14(9):932.
26. Hong JY, Kim H, Jeon WJ, Lee J, Ha IH. Elevated mitochondrial reactive oxygen species within cerebrospinal fluid as new index in the early detection of lumbar spinal stenosis. Diagnostics. 2021;11(5):748.
27. Rezaei B, Lotfi-Forushani H, Ensafi AA. Modified Au nanoparticles-imprinted sol–gel, multiwall carbon nanotubes pencil graphite electrode used as a sensor for ranitidine determination. Mater. Sci. Eng. C. 2014;37:113-9.
28. Brana C, Benham C, Sundstrom L. A method for characterising cell death in vitro by combining propidium iodide staining with immunohistochemistry. Brain Res. Brain Res. Protoc. 2002;10(2):109-14.
29. Li W, Li Y, Cui Y, Li S, Zhu Y, Shang C, Song G, Liu Z, Xiu Z, Cong J, Li T. Anti-tumour effects of a dual cancer-specific oncolytic adenovirus on Breast Cancer Stem cells. J Cell Mol Med. 2021;25(2):666-76.
30. Kazmi F, Hensley T, Pope C, Funk RS, Loewen GJ, Buckley DB, Parkinson A. Lysosomal sequestration (trapping) of lipophilic amine (cationic amphiphilic) drugs in immortalized human hepatocytes (Fa2N-4 cells). Drug Metab. Dispos. 2013;41(4):897-905.
31. Dong Z, Qiu T, Zhang J, Sha S, Han X, Kang J, Shi X, Sun X, Jiang L, Yang G, Yao X. Perfluorooctane sulfonate induces autophagy-dependent lysosomal membrane permeabilization by weakened interaction between tyrosinated alpha-tubulin and spinster 1. Food Chem. Toxicol. 2021;157:112540.
32. Han B, Baruah K, Cox E, Vanrompay D, Bossier P. Structure-functional activity relationship of β-glucans from the perspective of immunomodulation: a mini-review. Front. immunol. 2020;11:658.
33. Gani A, Ashraf ZU, Shah A, Noor N, Gani A. Encapsulation of vitamin D3 into β-glucan matrix using the supercritical carbon dioxide. ACS Food Sci. Technol. 2021;1(10):1880-7.
34. Shah A, ul Ashraf Z, Gani A, Masoodi FA, Gani A. β-Glucan from mushrooms and dates as a wall material for targeted delivery of model bioactive compound: Nutraceutical profiling and bioavailability. Ultrason Sonochem. 2022;82:105884.
35. ALTUĞ DT, ÇOLAK ÖF. Discrimination of Daedaleopsis nitida mushrooms that growing in different environments using fourier transform infrared spectroscopy. Sigma J. Engg and Nat Sc. 2018;36(2):577-82.
36. Sanpui P, Chattopadhyay A, Ghosh SS. Induction of apoptosis in cancer cells at low silver nanoparticle concentrations using chitosan nanocarrier. ACS Appl. Mater. Interfaces. 2011;3(2):218-28.
37. Kobayashi H, Yoshida R, Kanada Y, Fukuda Y, Yagyu T, Inagaki K, Kondo T, Kurita N, Suzuki M, Kanayama N, Terao T. Suppressing effects of daily oral supplementation of beta-glucan extracted from *Agaricus blazei* Murill on spontaneous and peritoneal disseminated metastasis in mouse model. J. Cancer Res. Clin. Oncol. 2005;131(8):527-38.
38. Sivandzade F, Bhalerao A, Cucullo L. Analysis of the mitochondrial membrane potential using the cationic JC-1 dye as a sensitive fluorescent probe. Bio-protocol. 2019;9(1):e3128-.
39. Tabata Y, Ikada Y. Macrophage phagocytosis of biodegradable microspheres composed of L-lactic acid/glycolic acid homo- and copolymers. J. Biomed. Mater. Res. 1988; 22(10):837-58.
40. Pillai TG, Maurya DK, Salvi VP, Janardhanan KK, Nair CK. Fungal beta glucan protects radiation induced DNA damage in human lymphocytes. Ann. Transl. Med. 2014;2(2).
41. Hassan AI, Ghoneim MA, Ibrahim RY. Therapeutic role of glucogalactan polysaccharide extracted from Agaricus bisporus on trimethyltin chloride induced neuropathy in rats. Afr. J. Biotechnol. 2015;14(24):2052-65.
42. Volman JJ, Ramakers JD, Plat J. Dietary modulation of immune function by β-glucans. Physiol. Behav. 2008;94(2):276-84.
43. Mahmoud Amer E, Saber SH, Abo Markeb A, Elkhawaga AA, Mekhemer IM, Zohri AN, Abujamel TS, Harakeh S, Abd-Allah EA. Enhancement of β-glucan biological activity using a modified acid-base extraction method from *Saccharomyces cerevisiae*. Molecules. 2021;26(8):2113.
44. Kiss A, Grünvald P, Ladányi M, Papp V, Papp I, Némedi E, Mirmazloum I. Heat treatment of Reishi medicinal mushroom (Ganoderma lingzhi) basidiocarp enhanced its β-glucan solubility, antioxidant capacity and lactogenic properties. Foods. 2021;10(9):2015.
45. Anjugam M, Vaseeharan B, Iswarya A, Divya M, Prabhu NM,

Sankaranarayanan K. Biological synthesis of silver nanoparticles using β-1, 3 glucan binding protein and their antibacterial, anti-biofilm and cytotoxic potential. Microb. Pathog. 2018;115:31-40.
46. Jurczyńska E, Saczko J, Kulbacka J, Kawa-Rygielska J, Błazewicz J. Beta-glukan, jako naturalny antykarcynogen [Beta-glucan as a natural anticancer agent]. Pol Merkur Lekarski. 2012;33(196):217-20. Polish. PMID: 23272610.
47. Wu L, Zhao J, Zhang X, Liu S, Zhao C. Antitumor effect of soluble β-glucan as an immune stimulant. Int. J. Biol. Macromol. 2021;179:116-24.
48. Kalafati L, Kourtzelis I, Schulte-Schrepping J, Li X, Hatzioannou A, Grinenko T, Hagag E, Sinha A, Has C, Dietz S, de Jesus Domingues AM. Innate immune training of granulopoiesis promotes anti-tumor activity. Cell. 2020;183(3):771-85.
49. Ma Z, Wang J, Zhang L, Zhang Y, Ding K. Evaluation of water soluble β-D-glucan from Auricularia auricular-judae as potential anti-tumor agent. Carbohydr. Polym. 2010;80(3):977-83.
50. Iuchi K, Ema M, Suzuki M, Yokoyama C, Hisatomi H. Oxidized unsaturated fatty acids induce apoptotic cell death in cultured cells. Mol. Med. Rep. 2019;19(4):2767-73.
51. Luzio JP, Pryor PR, Bright NA. Lysosomes: fusion and function. Nat. Rev. Mol. Cell Biol. 2007;8(8):622-32.
52. Platt FM, Boland B, van der Spoel AC. Lysosomal storage disorders: The cellular impact of lysosomal dysfunction. Int. J. Cell Biol. 2012;199(5):723-34.
53. Sinha SK, Upadhyay TK, Sharma SK. Nutritional-medicinal profile and quality categorization of fresh white button mushroom. Biointerface Res. Appl. Chem. 2021;11:8669-85.
54. Sinha SK, Upadhyay TK, Sharma SK. Heavy metals detection in white button Mushroom (Agaricus Bisporus) cultivatedin state of Maharashtra, India. Biochem Cell Arch. 2019;19:3501-6.